

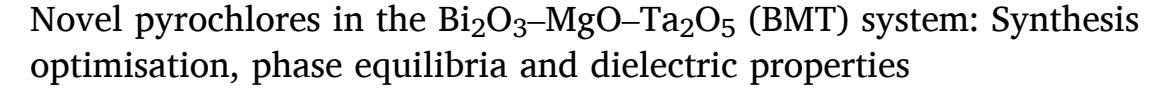
Contents lists available at ScienceDirect

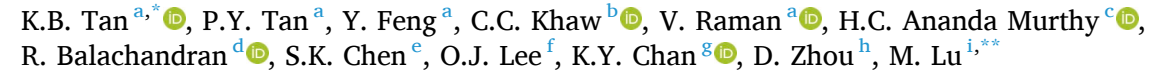
# Journal of Science: Advanced Materials and Devices

journal homepage: www.elsevier.com/locate/jsamd



### Research Article





- <sup>a</sup> Department of Chemistry, Faculty of Science, Universiti Putra Malaysia, UPM, Serdang, 43400, Selangor, Malaysia
- b Department of Mechanical and Material Engineering, Lee Kong Chian Faculty of Engineering and Science, Universiti Tunku Abdul Rahman, Bandar Sungai Long, 43000, Kajang, Selangor, Malaysia
- <sup>c</sup> Department of Prosthodontics, Saveetha Dental College and Hospital, Saveetha Institute of Medical and Technical Science (SIMATS), Saveetha University, Chennai, 600077, Tamil Nadu, India
- d Department of Electronics and Communication Engineering, Adama Science and Technology University, P.O. Box:1888, Adama, Ethiopia
- <sup>e</sup> Department of Physics, Faculty of Science, Universiti Putra Malaysia, UPM, Serdang, 43400, Selangor, Malaysia
- f Faculty of Science and Marine Environment, Universiti Malaysia Terengganu, Kuala Nerus, 21030, Terengganu, Malaysia
- g Centre for Advanced Devices and Systems, Faculty of Engineering, Multimedia University, Persiaran Multimedia, 63100, Cyberjaya, Selangor, Malaysia
- h Electronic Materials Research Laboratory, Key Laboratory of the Ministry of Education & International Center for Dielectric Research, School of Electronic Science and Engineering, Xi'an Jiaotong University, Xi'an, 710049, Shaanxi, China
- <sup>i</sup> Key Laboratory of Functional Materials Physics and Chemistry of the Ministry of Education, The Joint Laboratory of MXene Materials, Jilin Normal University, Changchun, 130103, Jilin, China

### ARTICLE INFO

#### Keywords: Phase equilibria Dielectrics Pyrochlores Tantalates

#### ABSTRACT

Investigating the phase equilibria within the  $Bi_2O_3$ –MgO–Ta<sub>2</sub>O<sub>5</sub> (BMT) system offers critical insights into the formation and stability of pyrochlore phases. This understanding enables the correlation of dielectric properties with phase equilibria data, facilitating the identification of compositions exhibiting optimal performance. Phase equilibria within the BMT system have been investigated across a temperature range of 800–1025 °C. The layouts of compatible triangles, encompassing two-phase, three-phase regions and the single-phase BMT subsolidus solution area, have been determined through qualitative XRD phase analysis of approximately 150 synthesised compositions. The BMT trapezoidal cubic pyrochlore region could be represented by the general formula of  $Bi_{3.56}$ -xMg<sub>1.96-y</sub>Ta<sub>2.48+x</sub> +  $_y$ O<sub>13.50+x+(3/2)y</sub>, 0.00  $\le$  x  $\le$  0.32; 0.00  $\le$  y  $\le$  0.20. Two formation mechanisms are proposed: (i) compositions of  $Bi_{3.56}$ -xMg<sub>1.96-y</sub>Ta<sub>2.48+x</sub>O<sub>13.50+x</sub> at fixed MgO content, involving a one-to-one substitution of  $Bi^{3+}$  by Ta<sup>5+</sup> and oxygen non-stoichiometry x  $Bi^{3+}$   $\rightarrow$  x Ta<sup>5+</sup> + x  $O^2$ - and (ii)  $Bi_{3.56}$ Mg<sub>1.96-y</sub>Ta<sub>2.48+y</sub>O<sub>13.50+(3/2)y</sub> at fixed bismuth content, with Mg content reduction proportional to Ta<sup>5+</sup> and  $O^2$ - substitution, i.e. y Mg<sup>2+</sup>  $\rightarrow$  y Ta<sup>5+</sup> + 3y/2  $O^2$ -. Dielectric properties within this extensive subsolidus solution area exhibit variability; specifically, BMT pyrochlores exhibit dielectric constants ( $\varepsilon$ ) ranging from 70 to 84, dielectric losses (tan  $\delta$ ) in the order of 0.2–9.1 × 10<sup>-3</sup>, negative temperature coefficients of dielectric constants (TC $\varepsilon$ ) ranging from 130 to 360 ppm/°C and activation energies (Ea) ranging from 1.10 to 1.48 eV.

### 1. Introduction

Advanced functional ceramics have garnered significant research interest due to their exceptional electrical properties. These materials find diverse applications, including electronic components, superconductors, sensors, capacitors and energy storage systems. Understanding the synthesis of these materials is crucial, as precise processing control is

essential to achieve chemical homogeneity and phase equilibria of the desired phases. To gain further insights into the relationship between composition, structure and properties of the prepared phases, a systematic characterisation using various spectroscopic, microscopic and physicochemical techniques is indispensable. Moreover, meticulous data interpretation is vital to exploring novel phases, optimising their properties and tailoring them into suitable forms before prototype

E-mail addresses: tankarban@upm.edu.my (K.B. Tan), kychan@mmu.edu.my (K.Y. Chan), zhoudi1220@xjtu.edu.cn (D. Zhou), luming@jlnu.edu.cn (M. Lu).

https://doi.org/10.1016/j.jsamd.2025.100866

Received 17 November 2024; Received in revised form 12 February 2025; Accepted 14 February 2025 Available online 19 February 2025

2468-2179/© 2025 Vietnam National University, Hanoi. Published by Elsevier B.V. This is an open access article under the CC BY license (http://creativecommons.org/licenses/by/4.0/).



<sup>\*</sup> Corresponding author.

<sup>\*\*</sup> Corresponding author.

testing for various applications [1,2].

Phase equilibria studies involve the coexistence of two or more phases in equilibrium, allowing for the prediction of phase stability based on the most stable material form. The phase diagram visually represents information on phase compatibilities, assemblages and thermal stabilities under chemical equilibrium conditions. Given the compositional and structural flexibility of pyrochlores, understanding their formation mechanisms and optimising their properties is crucial for specific applications. Specifically, their electrical properties, including oxide-ion conductivity, dielectric loss and temperature-independent relative permittivity, are tunable via compositional modification, facilitating the design of materials with precise property specifications [2].

Pyrochlore oxides, expressed by the formula  $A_2B_2O_7$ , possess two distinct crystallographic sites: an 8-coordinate A site and a 6-coordinate B site. These sites are typically occupied by combinations of  $A^{3+}$  and  $B^{4+}$  cations,  $A^{2+}$  and  $B^{5+}$  cations, or other combinations that achieve the required average mixed valency [3–6]. The numerous possible substitutions for A and B sites result in a wide range of interesting properties exhibited by these pyrochlore oxides. Our prior research, along with the studies by other research groups [5,7–15], on the  $Bi_2O_3$ –ZnO– $Nb_2O_5$  ternary system has revealed that the phase with the composition,  $Bi_{1.5}Zn_{0.692}Nb_{1.5}O_7$  exhibits exceptional dielectric properties, suggesting its potential application in multilayered ceramic capacitors (MLCC). Moreover, the  $\epsilon'$  of this phase exhibits a strong dependence on temperature. Reducing this dependence is highly desirable, as it enables additional applications, such as low  $TC\epsilon'$  for ceramic capacitors [8,12–14].

The prior research has demonstrated that a diverse range of dopants, including M' = Zn, Mg, Ni, Ca, Cu and Fe, and M'' = Nb, Ta and Sb, could be introduced into the  $(Bi_{1.5}M_{0.5}')(M_{0.5}'M_{1.5}'')O_7$  and  $Bi_2(M_{2/3}'M_{4/3}'')_2O_7$ systems [10,11,15–26]. In addition to the  $A_2B_2O_7$  pyrochlores, trivalent metal cations may also occupy the B site and this has been reported in the  $Bi_2MNbO_7$  ( $M^{3+}$  = Fe, In and Sc) systems. However, many other phases prepared through various chemical doping and/or methods were not included in these studies. Given the close similarities in ionic radii and electronic shell configurations, Cu-substituted  $\alpha$ -phases in the analogous Bi<sub>2</sub>O<sub>3</sub>-CuO-Ta<sub>2</sub>O<sub>5</sub> (BCT) ternary system were successfully synthesised and characterised [21,25]. Our phase diagram studies [7,9, 24-26] revealed common resemblances, as α-phases in both the Zn- and Cu-analogues could form over a broad subsolidus area, except the latter was found in a slightly lower bismuth region. Notably, the ternary phase diagram in the Zn-analogue also involves an α-phase of nominal stoichiometry,  $(Bi_{1.5}Zn_{0.5})(Zn_{0.5}Ta_{1.5})O_7$  as the pivotal composition for the explanation of subsolidus mechanisms. Concurrently, the structurally related β-phase, Bi<sub>2</sub>(Zn<sub>1/3</sub>Ta<sub>2/3</sub>)<sub>2</sub>O<sub>7</sub>, appeared to possess a variable composition that, to date, remains inadequately characterised [26].

Consequently, extensive efforts have been devoted to introducing a diverse range of divalent cations into  ${\rm Bi_2O_3\text{-}MO\text{-}Ta_2O_5}$  systems, where cation M can be alkaline earth metals (Mg, Sr and Ca) and/or transition divalent metals (Co, Mn, Fe, Ni and Cu) of the late period 3d elements [1, 16,25,27-34]. This approach has led to the discovery of numerous novel phases in Bi-pyrochlore systems. Interestingly, the incompatible M divalent cations, which possess relatively small ionic radii for an eight-coordinate A site, do not appear to pose a significant impediment to the formation of new pyrochlores [35]. The presence of small divalent cations at the A site, as calculated through bond valence sum analysis (BVS) and Monte Carlo simulation [5,15], may contribute to structured diffuse scattering and/or local short-range order in the  $\rm A_2O(2)$  substructure.

Given the inconsistencies and discrepancies in the literature, a comprehensive phase equilibria study of the bismuth magnesium tantalate (BMT) system is crucial due to the complex structure, variable stoichiometry and intriguing dielectric properties of pyrochlore. This study will address the following objectives: (i) determination of optimal synthesis conditions for BMT subsolidus pyrochlores and related phases; (ii) investigation of phase assemblages and compatibilities within the

BMT system; and (iii) qualitative discussion of subsolidus formation mechanisms and the variation of dielectric properties in BMT cubic pyrochlores.

### 2. Experimental

Various binary and ternary phases with varying cation ratios in the Bi<sub>2</sub>O<sub>3</sub>-MgO-Ta<sub>2</sub>O<sub>5</sub> (BMT) system were synthesised via solid-state reaction. Prior to sample preparation, the reagent grade oxides, including Bi<sub>2</sub>O<sub>3</sub> (Alfa Aesar, 99.99%), MgO (Aldrich, 99+%) and Ta<sub>2</sub>O<sub>5</sub> (Alfa Aesar, 99.99%), underwent pre-heat treatment. Bi2O3 was heated at 300 °C, while the other two oxides were heated at 600 °C for 3 h to eliminate moisture and impurities. The reactants, totalling approximately 3-4 g, were precisely weighed, homogeneously ground in sufficient acetone and loaded into a platinum boat before being fired at temperatures ranging from 700 to 1050 °C. A meticulous heat treatment protocol was implemented, starting with lower temperatures in stages to facilitate the initial reaction of  $Bi_2O_3$  below 800 °C. The optimal synthesis temperature required to achieve equilibrium was carefully determined through an iterative process, gradually decreasing from approximately 1050 °C for compositions with higher bismuth content. Notably, certain samples within the bismuth-rich region necessitated preparation at lower sintering temperatures, specifically below 900 °C, to mitigate potential bismuth volatilisation. To ensure thermal equilibrium, the samples were subjected to repeated heating cycles until no further phase changes were observed, either at the same temperature or upon incremental temperature increases of 25-50 °C. In other words, a stringent control over the firing process is paramount in establishing experimental conditions that facilitate complete chemical reactions and yield final products representing the most thermally stable form.

Approximately 150 compositions were meticulously synthesised using the aforementioned methodology and their phase purities were rigorously assessed employing a Shimadzu X-ray diffractometer equipped with CuK $\alpha$  radiation. The diffraction data were collected at  $2^{\circ}$  steps from  $10^{\circ}$  to  $70^{\circ}$  20. The phase compatibility and assemblages across the BMT composition range were determined using the Gibbs' disappearing phase method. The stoichiometry of phase-pure pyrochlores was determined via inductively coupled plasma optical emission spectroscopy (PerkinElmer ICP-OES, Optima DV 2000) using triplicate samples  $(0.1 \text{ g dissolved in } 250 \text{ ml of } 5\% \text{ HNO}_3 \text{ and HF})$ . The thermal stability of phase-pure BMT pyrochlores was investigated using thermal gravimetric and differential thermogravimetric analysis (PerkinElmer, STA 6000) from 28 °C to 1000 °C at 10 °C/min under nitrogen. The electrical characterisation followed the optimisation procedure in Ref. [26]. Selected phase-pure pyrochlores were pelletised, densified and gold-coated before electrical measurements using an AC impedance analyser (Hewlett-Packard, HP4192A) from 5 Hz to 13 MHz and 25 °C-850 °C.

#### 3. Results and discussion

### 3.1. Phase diagram of Bi<sub>2</sub>O<sub>3</sub>-MgO-Ta<sub>2</sub>O<sub>5</sub> (BMT) ternary system

A thorough investigation of the binary joins of the  $Bi_2O_3$ – $MgO-Ta_2O_5$  (BMT) ternary system is essential before constructing the comprehensive phase diagram. The BMT ternary system comprises three distinct binary joins:  $Bi_2O_3-Ta_2O_5$ ,  $MgO-Ta_2O_5$  and  $Bi_2O_3-MgO$ , respectively. Within the  $Bi_2O_3-Ta_2O_5$  binary join, various phases have been identified, including  $Bi_3TaO_7$ ,  $Bi_7Ta_3O_{18}$ ,  $Bi_4Ta_2O_{11}$ ,  $BiTaO_4$  and  $BiTa_7O_{19}$ . To validate their existence, these phases were synthesised within a temperature range of 800 °C–1025 °C and found to be thermal stability. Notably, at bismuth concentrations exceeding 75 mol % of  $Bi_2O_3$ , a fluorite-related structured phase forms an extensive range of subsolidus solution [36,37]. Conversely, while  $Bi_4Ta_2O_{11}$  was initially reported as a single-phase compound along the  $Bi_7Ta_3O_{18}$  and  $BiTaO_4$  tie line, our analysis reveals it to be a multi-phase material containing

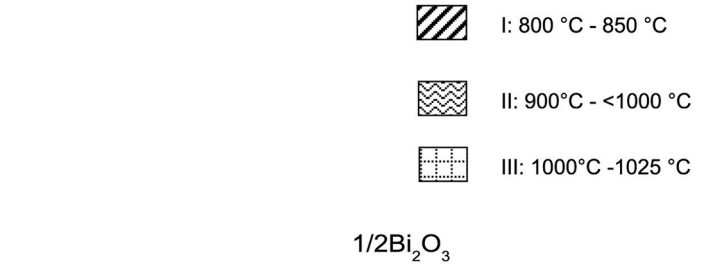
the aurivillius-structured  $Bi_{31}Ta_{17}O_{89}$  phase. Nevertheless, its X-ray diffraction pattern exhibits strong similarity to that of  $Bi_7Ta_3O_{18}$ . This is consistent with prior research indicating the formation of an additional phase above 1000 °C [37].

In the binary join of MgO-Ta<sub>2</sub>O<sub>5</sub>, an early literature review suggested that two distinct phases were identified: trirutile structure, MgTa<sub>2</sub>O<sub>6</sub> and corundum structure, Mg<sub>4</sub>Ta<sub>2</sub>O<sub>9</sub> [38]. These phases exhibited stability at temperatures as low as 750 °C and melted at 1800 °C and 1810 °C, respectively. A third phase, Mg<sub>3</sub>Ta<sub>2</sub>O<sub>8</sub> with a rhombic unit cell, existed only within a narrow high-temperature range of 1475–1675 °C. This phase may decompose into a mixture of MgTa<sub>2</sub>O<sub>6</sub> and Mg<sub>4</sub>Ta<sub>2</sub>O<sub>9</sub> phases at lower temperatures due to its lower limit of stability [39]. Additionally, a pyrochlore-like phase, Mg<sub>2</sub>Ta<sub>2</sub>O<sub>7</sub> with a ratio of 2 MgO: Ta<sub>2</sub>O<sub>5</sub>, was successfully quenched from higher temperatures, i.e. 1400-1600 °C [40]. Nevertheless, both Mg<sub>3</sub>Ta<sub>2</sub>O<sub>8</sub> and Mg<sub>2</sub>Ta<sub>2</sub>O<sub>7</sub> phases would undergo thermal decomposition and are therefore excluded as metastable phases. In the binary join of Bi<sub>2</sub>O<sub>3</sub>. -MgO, a single binary phase with the formula Bi<sub>12</sub>MgO<sub>19</sub> has been reported. However, this phase is not included in our diagram due to its high formation temperature above 1100 °C [41].

Following the confirmation of various binary phases, the subsequent task is to ascertain the phase compatibilities and assemblages of various phases within the BMT system. Technically, the BMT phase diagram can be categorised into three isothermal regions (Fig. 1). Each region is demarcated by a tie line between two phases encompassing  $\rm Bi_3TaO_7$ –MgO,  $\rm Bi_3TaO_7$ -cubic pyrochlore and cubic pyrochlore-MgO, respectively. The region I represents a high bismuth content region, segregated from the region II by the  $\rm Bi_3TaO_7$ –MgO tie line. The sample preparation is conducted within the temperature range of 800–850 °C.

In order to prevent potential partial melting or excessive bismuth loss during the high-temperature firing process, it is crucial to consider the low melting point of  $\rm Bi_2O_3$  (825 °C) [42]. Meanwhile, the regions II and III in the BMT ternary phase diagram are divided by the tie lines of  $\rm Bi_3TaO_7$ -cubic pyrochlore and MgO-cubic pyrochlore. The sample synthesis was performed at temperatures ranging from 900 °C to just below 1000 °C. The compositions in this region fail to reach thermal equilibrium at temperatures below 900 °C; however, they will begin to melt or experience significant weight loss (greater than 2%) if the temperature exceeds 1000 °C. The region III is characterised by a low bismuth content. The compositions in this region are synthesised within the temperature range of 1000–1025 °C and exhibit exceptional thermal stability due to the highly refractory properties of MgO (~2827 °C) [43] and  $\rm Ta_2O_5$  (~1872 °C), respectively [44].

Within the Region III, there are several two-phase and three-phase assemblages. Specifically, there are four two-phase and seven three-phase assemblages in this region. The samples in two-phase assemblages are predominantly characterised by the presence of a ternary homogeneity region of pyrochlore, which is compatible with other binary phases such as  $\rm Bi_7Ta_3O_{18}$  and  $\rm BiTaO_4$ . In contrast, the compositions in the three-phase assemblages primarily consist of two binary phases and a compatible ternary pyrochlore phase. These phases are found within the regions of cubic pyrochlore-Bi\_3TaO\_7-Bi\_7Ta\_3O\_{18}, cubic pyrochlore-Bi\_7Ta\_3O\_{18}-BiTaO\_4, cubic pyrochlore-Bi\_3TaO\_4-MgTa\_2O\_6 and cubic pyrochlore-MgTa\_2O\_6-Mg\_4Ta\_2O\_9, respectively. In this study, the arrangement of compatible triangles, encompassing two-phase or three-phase regions along with the single-phase solid solution area in the BMT ternary system, has been established. Furthermore, the phase relationships for approximately 150 compositions are in complete agreement



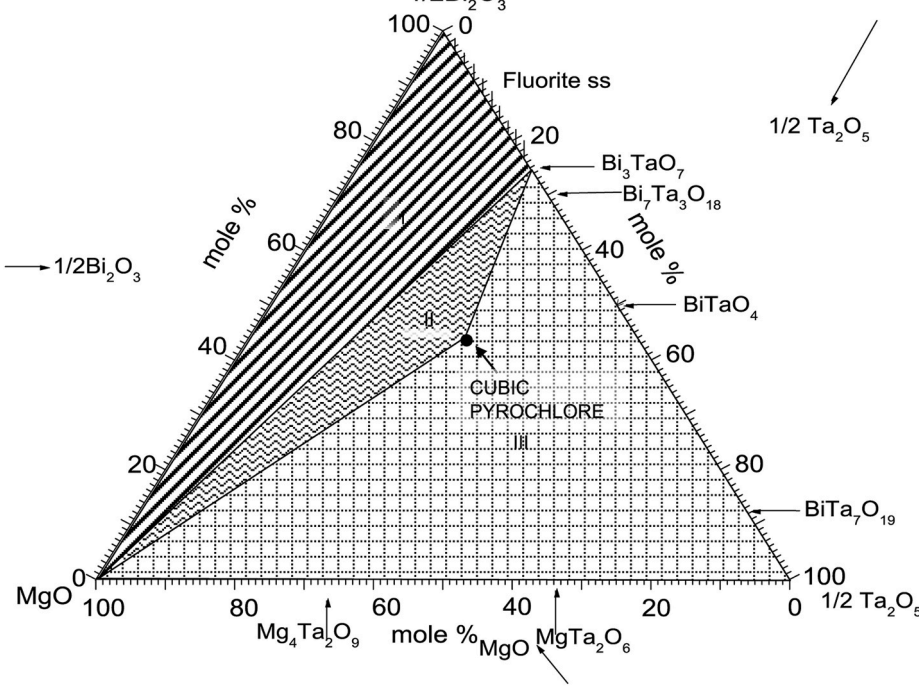


Fig. 1. The isothermal regions in Bi<sub>2</sub>O<sub>3</sub>–MgO–Ta<sub>2</sub>O<sub>5</sub> ternary system.

with the results presented in Supporting Information, Table I. The comprehensive phase diagram and expanded subsolidus solution of the BMT system are depicted in Figs. 2 and 3, respectively.

#### 3.2. Cubic pyrochlore homogeneity range and doping mechanisms

Single-phase cubic pyrochlores in the BMT ternary system are formed in the bismuth-rich region, i.e., compositions with approximately 40.5–44.5 mol % Bi at a firing temperature of 1025 °C over 48 h. The subsolidus solution area is clearly delineated by a trapezoidal area wherein two of the four edges are parallel with constant MgO contents of 22.0 mol % and 24.5 mol % (Fig. 3; expanded magenta triangular region in Fig. 2). Meanwhile, the chemical stoichiometries of the phase pure BMT pyrochlore, as determined by ICP-OES, are found to be in good agreement to those calculated values with no evidence of any systematic deviation from stoichiometry; specifically, loss of Bi<sub>2</sub>O<sub>3</sub> is not a problem (Supporting information, Table II). The combined thermal analyses also confirm that the BMT pyrochlores are thermally stable and impervious to any thermal events over the studied temperature range, i.e.  $\sim$ 28–1000 °C (Supporting Information, Figs. I and II).

It is noteworthy that the subsolidus area of the BMT ternary system is relatively smaller than those of other reported Nb pyrochlore analogues,  $\mathrm{Bi}_2\mathrm{O}_3\text{-}M\text{-}\mathrm{Nb}_2\mathrm{O}_5$  (M =  $\mathrm{Mn}_2\mathrm{O}_3$ , Fe\_2O\_3, CoO, NiO, CuO and ZnO) [7,19,20, 22–24]. In comparison to our previous studies, the BMT pyrochlores form a trapezoidal area similar to that of the  $\mathrm{Bi}_2\mathrm{O}_3\text{-}Zn\mathrm{O}\text{-}\mathrm{Ta}_2\mathrm{O}_5$  (BZT) system [9,26]. However, the subsolidus area of the BMT ternary system is found to be located in the higher bismuth content region. The pyrochlore formation with different solid solution ranges could be influenced by the electronic structure and/or size of the constituent elements. Furthermore, the location of the pyrochlore region could be affected by the sinterability, particularly due to the highly volatile bismuth. In this context, Mn, Fe, Co, and Ni are transition metals with unpaired d orbital electrons at the high spin state, enabling them to adopt various coordination environments. Consequently, this allows them to exhibit greater tolerance towards bismuth solubilities as these transition metals

can occupy randomly either the A sites or B sites of the pyrochlore structure. Both the reported BZN and BZT pyrochlore systems demonstrated a relatively larger pyrochlore subsolidus area than the respective Mg analogues [9,26]. This may be attributed to the 3d orbital of Zn, which could establish an energetically stable asymmetric crystal field potential. Consequently, the coordination ability is less restricted, resulting in a higher tolerance for bismuth solubility. In contrast, Mg cannot form any asymmetric bonds due to its rigid electron orbital shell and lacks of the d orbital like other divalent cations. Therefore, the BMT system exhibits the smallest variation in Bi content and solid solution area compared to other analogous Bi-pyrochlore ternary systems (Fig. 4) [7,19,20,22-26]. On the other hand, the firing temperature is also significantly influenced by the bismuth content, as substantial bismuth loss could occur at high temperatures. The phase-pure BMT pyrochlores can withstand high firing temperatures, i.e., 1025 °C, without showing any significant bismuth weight loss. This can be attributed to the high refractory and unreactive nature of MgO, which has an exceptionally high melting point of 2827 °C.

In overall, the BMT subsolidus cubic pyrochlore area could be best described using two compositional variables, x and y, as illustrated in Fig. 5. The phase-pure pyrochlore, Bi<sub>3.56</sub>Mg<sub>1.96</sub>Ta<sub>2.48</sub>O<sub>13.50</sub> (P2, sample 129), serves as the reference point for further analysis. The XRD data for this composition are comprehensively indexed, as summarised in Table 1. Two distinct formation mechanisms are proposed: (i) Bi<sub>3.56</sub>xMg<sub>1.96</sub>Ta<sub>2.48+x</sub>O<sub>13.50+x</sub> compositions with a fixed MgO content (samples 129, 99, 92, 94, and 96; Fig. 5). This mechanism involves a one-toone replacement of Bi<sup>3+</sup> by Ta<sup>5+</sup> accompanied by a variation in oxygen content, represented as x Bi<sup>3+</sup>  $\rightarrow$  x Ta<sup>5+</sup> + x O<sup>2-</sup>. The substitution of a lower valence cation (Bi<sup>3+</sup>) by a higher valence cation (Ta<sup>5+</sup>) is likely compensated by the creation of oxygen interstitialcies to maintain charge neutrality. (ii)  $Bi_{3.56}Mg_{1.96-y}Ta_{2.48+y}O_{13.50+(3/2)y}$  compositions (samples 129, 89, 88, and 68; Fig. 5). This mechanism involves a fixed bismuth content, wherein a reduction in Mg content is accompanied by an increased proportion of  $Ta^{5+}$  and  $O^{2-}$ , represented as  $y Mg^{2+} \rightarrow y$  $Ta^{5+} + {}_{3v/2} O^{2-}$ . By combining these mechanisms, the overall BMT

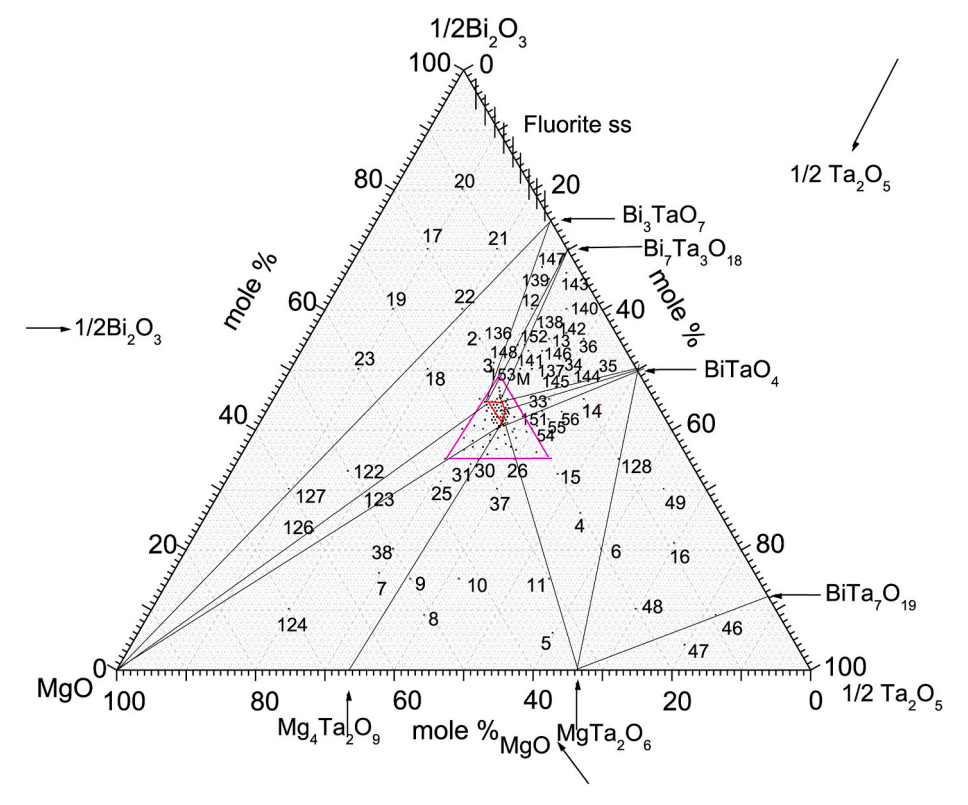


Fig. 2. The subsolidus phase diagram of the Bi<sub>2</sub>O<sub>3</sub>-MgO-Ta<sub>2</sub>O<sub>5</sub> ternary system.

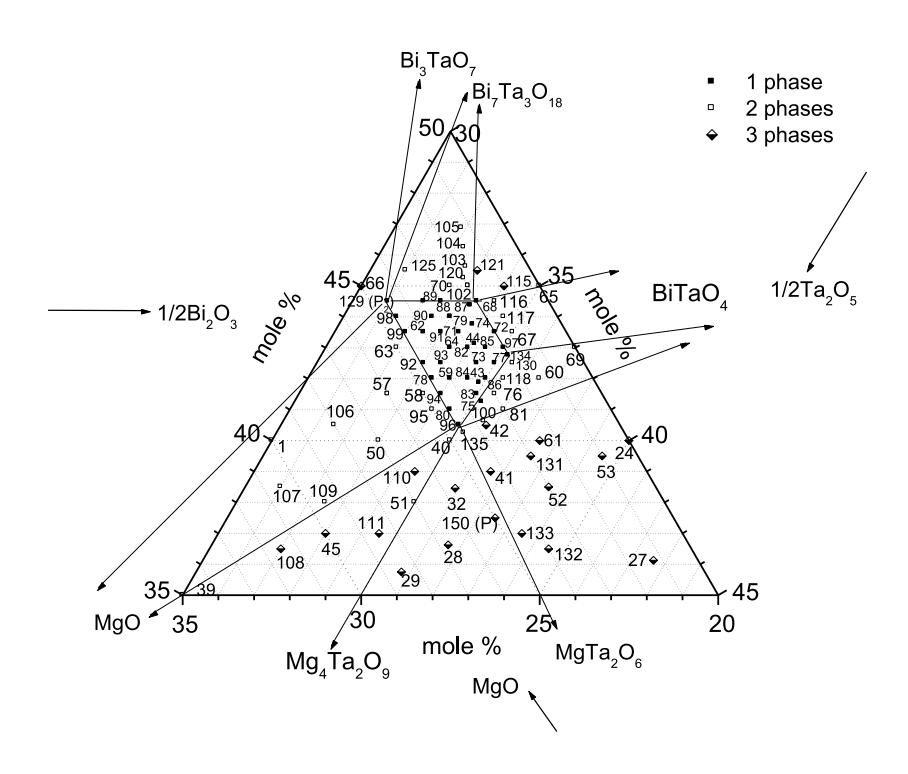
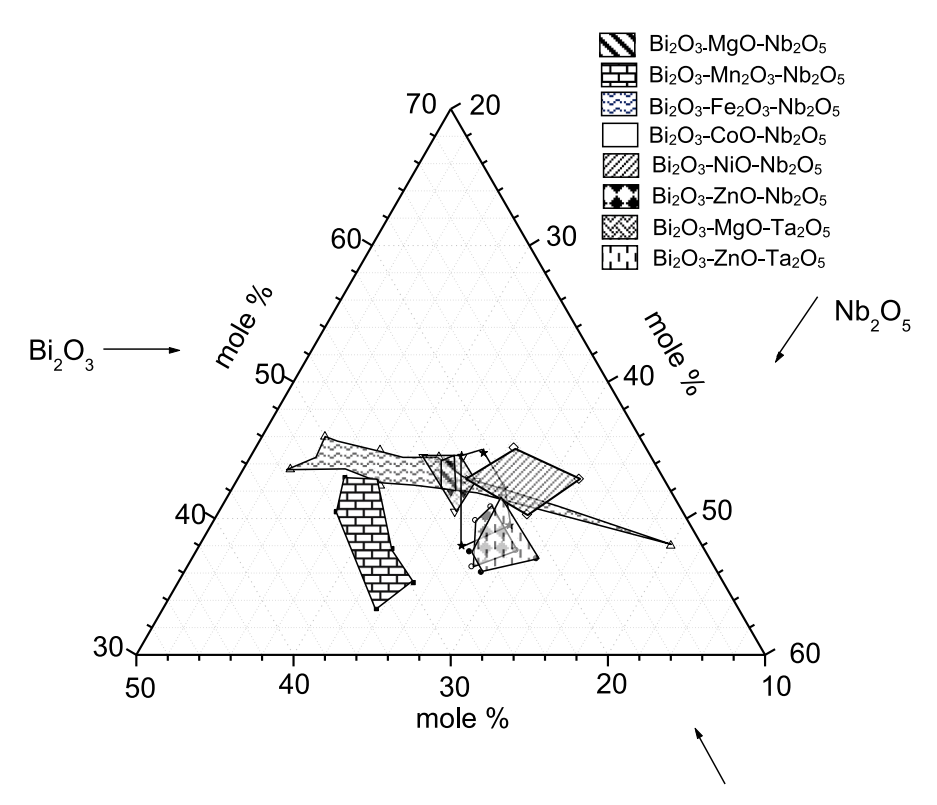


Fig. 3. The expanded subsolidus phase diagram of the  $Bi_2O_3$ -MgO-Ta $_2O_5$  ternary system.



 $\textbf{Fig. 4.} \ \ \text{The subsolidus cubic pyrochlore areas of the different } \ Bi_2O_3-M-Nb_2O_5/Ta_2O_5 \ (M=MgO,\ Mn_2O_3,\ Fe_2O_3,\ Co_2O_3,\ NiO,\ ZnO) \ \text{ternary systems.}$ 

subsolidus pyrochlore area can be represented by the general formula of  $Bi_{3.56\text{-}x}Mg_{1.96\text{-}y}Ta_{2.48+x}+_yO_{13.50+x+(3/2)y},$  where  $0.00 \leq x \leq 0.32$  and  $0.00 \leq y \leq 0.20,$  respectively. When comparing the pyrochlore subsolidus areas of the BMT and BZT ternary systems, they are significantly

narrower than the corresponding niobate analogues [9,26]. Furthermore, Nb and Ta are isomorphous and have the same ionic radii due to lanthanide contraction effect, these Ta and Nb pyrochlore analogues are expected to have a comparable size of the pyrochlore region. Without

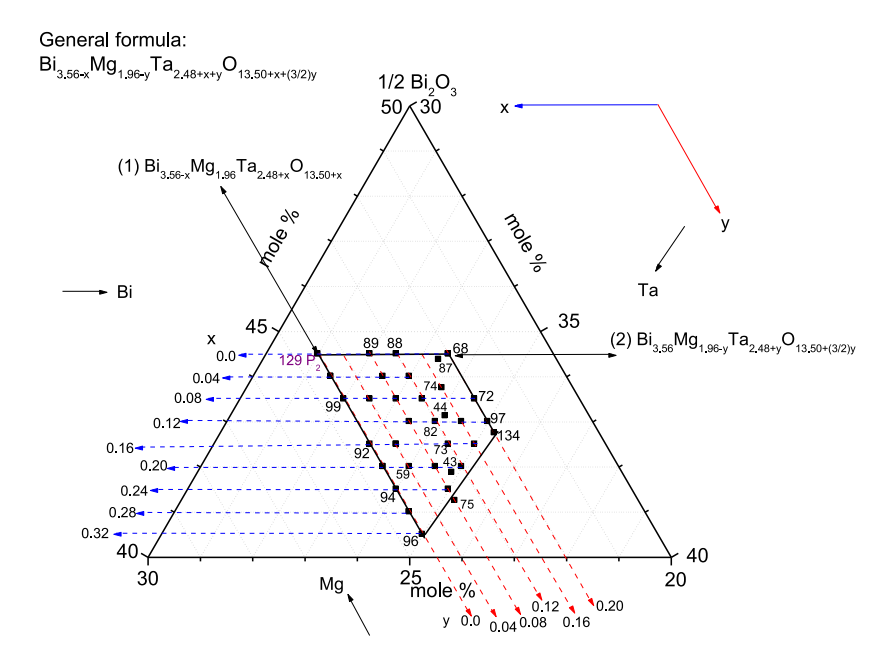


Fig. 5. The superposed BMT pyrochlore subsolidus solution area on the compositional grid with x and y variables using the proposed formula of  $Bi_{3.56-x}Mg_{1.96-y}Ta_{2.48+x+y}O_{13.50+x+(3/2)y}$ .

 $\label{eq:Table 1} \begin{array}{llll} \textbf{Table 1} \\ \textbf{The indexed X-ray diffraction pattern of Bi}_{3.56} Mg_{1.96} Ta_{2.48} O_{13.50} & cubic pyrochlore. \end{array}$ 

Refined lattice parameter									
a: 10.561	a: 10.5614(10) Å								
α: 90°									
Volume:	1178.04(33) Å <sup>3</sup>								
hkl	I/I <sub>0</sub>	d (obs) (Å)	d (calc) (Å)	Δ (2θ)					
111	1	6.0836	6.0976	0.034					
220	1	3.7293	3.7340	0.031					
131	1	3.1888	3.1844	-0.040					
222	100	3.0422	3.0488	0.045					
400	29	2.6377	2.6403	0.035					
313	2	2.4245	2.4229	-0.024					
242	1	2.1543	2.1558	0.031					
333	1	2.0333	2.0325	-0.018					
404	37	1.8661	1.8670	0.026					
244	1	1.7617	1.7602	-0.047					
620	1	1.6701	1.6699	-0.007					
622	34	1.5918	1.5922	0.014					
444	9	1.5243	1.5244	0.005					
551	1	1.4784	1.4789	0.025					
264	1	1.4112	1.4113	0.004					
535	1	1.3761	1.3750	-0.064					

additional crystallographic information on the specific mechanisms responsible for stabilising the pyrochlore structure, the reasons for this anomaly remain unclear.

## 3.3. Dielectric properties of BMT cubic pyrochlore solid solutions

The detailed descriptions of AC impedance characterisation and electrical circuit fitting studies covering both low and high temperatures of BMT pyrcohlores could be found in Refs. [29,45]. Three BMT subsolidus solution series, Bi<sub>3.56-x</sub>Mg<sub>1.96-y</sub>Ta<sub>2.48+x</sub> +  $_{y}$ O<sub>13.50+x+(3/2)y</sub> (SS3; x = 0.01, 0.06, 0.11, 0.16, 0.21 and 0.26; y = 0.18, 0.16, 0.14, 0.12, 0.10 and 0.08), Bi<sub>3.56-x</sub>Mg<sub>1.96-y</sub>Ta<sub>2.48+x</sub> +  $_{y}$ O<sub>13.50+x+(3/2)y</sub> (SS4; y = 0.00; 0.00

 $\leq$  x  $\leq$  0.32) and Bi\_{3.56}Mg\_{1.96\text{-yTa2.48+y}}O\_{13.50+3\text{y/2}} (SS5; x = 0.00; 0.00  $\leq$ y < 0.20) are utilised to investigate the electrical properties of BMT pyrochlores at elevated temperatures. The Arrhenius conductivity plots (not shown herewith) showed these BMT pyrochlores exhibit a reversible behaviour over heat-cool cyles with activation energies ranging from 1.17 to 1.49 eV (Fig. 6a). Notably, a high activation energy, exceeding 1.0 eV, is obtained and this elevated value is typically associated with a hopping-type electronic transport mechanism, provided it is not linked to ionic conduction [8,9,26]. On the other hand, the high activation energy also suggests that these BMT pyrochlores are highly insulating whose electrical conducvitities are to be measurable accurately at higher temperatures, i.e., above 550 °C. It has been suggested that the activation energy in relaxor materials may reduce by a larger volume of the coherent polarising unit [13,35]. It is anticipated that the higher coherent polarisation volume would result from fewer local symmetry disruptions that caused by the reduction of Mg at the A site in the BMT cubic pyrochlores. However, there is no discernible systematic shift in the activation energies of these BMT samples and comparable outcomes are observed in the BMN cubic pyrochlores [9,10,29,45]. This could be attributed to a minor variation in Mg and Bi occupancy at the A site. The activation energies for these samples are comparable to those of  $Bi_3Zn_2Sb_3O_{14}$  (BZS),  $Bi_3Zn_2Nb_3O_{14}$  (BZN) and  $Bi_3Zn_2Ta_3O_{14}$  (BZT), with activation energies of 1.36 eV,  $\sim$ 1.59 eV and 1.55 eV, respectively [9,10, 29,46].

The variation of dielectric properties of compositions in the BMT pyrochlore subsolidus solution area is illustrated in Fig. 6b–d. The BMT pyrochlores exhibit  $\epsilon'$  values ranging from 73 to 84 and tan  $\delta$  values in the order of  $10^{-3}$ , as measured at room temperature and a fixed frequency of 1 MHz. Fig. 6b shows the temperature dependence of dielectric constant,  $\epsilon'$  of the prepared SS3, SS4 and SS5 pyrochlore series. For the SS3 series, Bi\_3.56-xMg\_1.96-yTa\_2.48+x+yO\_{13.50+x+(3/2)y}, the  $\epsilon'$  values are found to increase with decreasing x values. The dielectric constant of materials is influenced by the dielectric polarisation from ions, electrons and defect structures within a material. Notably, the cations occupying different sites have different ionic radii and polarisability. The high polarisability,  $\alpha$  of Bi $^3+$  ( $\alpha=6.12$   $^3$ ) facilitates the polarisation process,

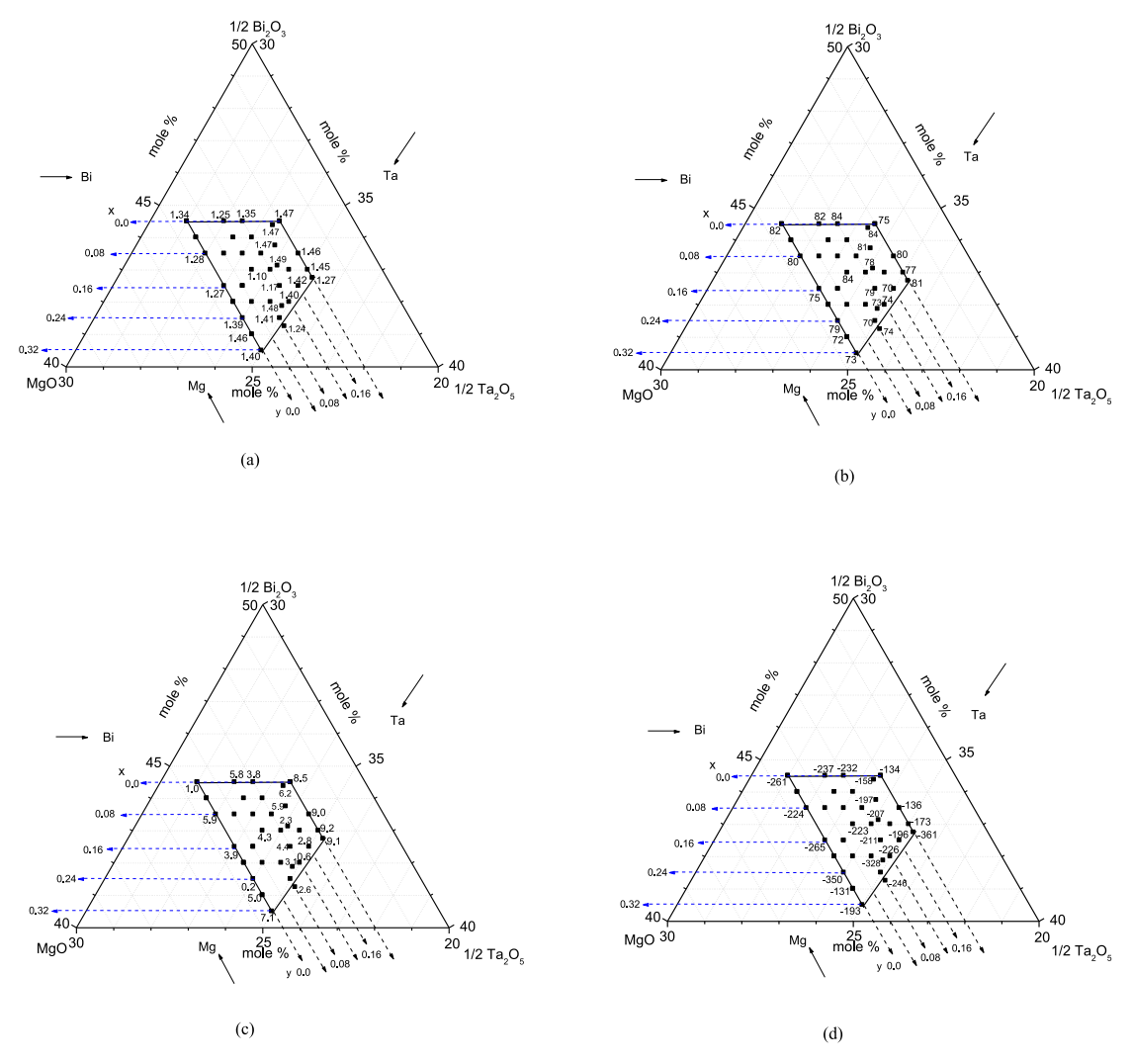


**Fig. 6.** The variations of dielectric properties of phase pure BMT pyrochlores at a fixed frequency of 1 MHz and room temperature: (a) activation energy (b) dielectric constant, (c) dielectric loss (in the order of  $10^{-3}$ ) and (d)  $TC\epsilon'$ 

thus contributing to the high dielectric constant [35]. For the SS4 series,  $Bi_{3.56\text{-}x}Mg_{1.96\text{-}y}Ta_{2.48+x}+yO_{13.50+x+3y/2}$  compositions have a fixed Mg content and exhibit a slight decrease in  $\epsilon'$  as x increases. This decrease is attributed to the reduction in the total polarisation volume of  $Bi^{3+}$ . However, no clear trend is observed in the  $\epsilon'$  values for the SS5 series,  $Bi_{3.56\text{-}x}Mg_{1.96\text{-}y}Ta_{2.48+x}+yO_{13.50+x+3y/2}.$  On a separate note, the dielectric losses in all BMT pyrochlores are found to be relatively low and this may attribute to the MgO, which serves to prevent high thermal loss during electrical conduction. Typically, the temperature dependence of  $\epsilon'$  and  $\tan\delta$  is attributed to the polarisation effect. The number of space-charge carriers governing space-charge polarisation tends to increase with rising temperature. This phenomenon leads to stronger polarisation, particularly in dielectric materials [8–10,46],

The temperature coefficient of relative permittivity (TC $\epsilon'$ ) of BMT pyrochlores was measured between approximately ~28–300 °C at a frequency of 1 MHz. The TC $\epsilon'$  values for the pyrochlores for SS3, SS4 and SS5 series were calculated from the gradient of the  $\epsilon'$  versus temperature plots. The BMT pyrochlores exhibited negative TC $\epsilon'$  values ranging from 158 ppm/°C to 358 ppm/°C (Fig. 6d). These values are comparable to those of cubic BZT pyrochlores, whose reported negative values are between 156 and 183 ppm/°C. However, the TC $\epsilon'$  values for the BMT pyrochlores are generally less negative than those of BMN pyrochlores,

which have negative TC $\epsilon'$  values of 528–742 ppm/°C. The difference in TC $\epsilon'$  values between Nb and Ta pyrochlores is attributed to the strength of the correlation between the B ions located at the center of the octahedra, BO $_6$ . Nonetheless, there is no apparent correlation between TC $\epsilon'$  values and the changing cation ratio in this study. The sumamry of dielectric properties of the BMT pyrochlores are included in Table 2.

In the BMT pyrochlore,  ${\rm Mg}^{2+}$  cations are likely distributed randomly over both A and B sites, with a general formula of (Bi<sub>3.56</sub>Mg<sub>0.44</sub>) (Mg<sub>1.52</sub>Ta<sub>2.48</sub>)O<sub>13.50</sub>. Either of the crystallographic A- or B- sites could be responsible for the polarity of the crystal structure and potential nanodomain formation. The eight-coordinate A site contains two ions, Bi<sup>3+</sup> and Mg<sup>2+</sup>, with significantly different sizes and coordination requirements, suggesting the possibility of off-center displacement of the smaller Mg<sup>2+</sup> ions. Similarly, the octahedral B site also contains a mixture of two ions, Mg<sup>2+</sup> and Ta<sup>5+</sup> with varying sizes and charges. From our published results, the polarisation with mixed occupancy of octahedral sites at B-site may behave similar to the established Nb-pyrochlore analogues or even the perovskite structure of PMN, lead magnesium niobate [45,47–49]. A third possibility is that one of the oxygen sites, often denoted as O', exhibits positional disorder in pyrochlores and could contribute to polarisation.

On the other hand, it is possible that the three polarisation processes

**Table 2**The summary of the dielectric properties of the BMT pyrochlores.

SS3 (x/y)	$\epsilon'$	$ an \delta$	TCe', ppm/°C (~30 °C–300 °C)	Ea, eV
0.26/0.08	74	0.0026	-246	1.24
0.21/0.10	73	0.0031	-328	1.48
0.16/0.12	79	0.0044	-211	1.17
0.11/0.14	78	0.0023	-207	1.49
0.06/0.16	81	0.0059	-197	1.47
0.01/0.18	84	0.0062	-158	1.47
SS4 (x; $y = 0$	)			
0.00	82	0.0010	-261	1.34
0.08	80	0.0059	-224	1.28
0.16	75	0.0039	-265	1.27
0.24	79	0.0002	-350	1.39
0.32	73	0.0071	-193	1.40
SS5 (x = 0; y	)			
0.00	82	0.0010	-261	1.34
0.08	82	0.0058	-237	1.25
0.12	84	0.0038	-232	1.35
0.20	75	0.0085	-134	1.47

mentioned contribute to the low-temperature relaxor properties and these processes may interact cooperatively to form polar domains. For example, the relaxation could be a result of the hopping of dynamically disordered A site cations and O' ions among the closely spaced possible positions. The relative interaction between the cations at the disordered A sites (Mg<sup>2+</sup> and Bi<sup>3+</sup>) and the O' ions would form unstable dipoles within the pyrochlore structure [47-49]. Therefore, the dielectric relaxation is possibly formed due to the reorientation of the dipoles under external ac fields. Meanwhile, the inhomogeneous distribution of Mg<sup>2+</sup> in the pyrochlore structure also may introduce more random fields. This could yield multiwell potentials that have a wide distribution of heights, necessitating the different transition rates, for Bi<sup>3+</sup> and Mg<sup>2+</sup> cations. Such interatomic potential can cause a broad dielectric relaxation [13,50]. However, cooperative alignment within domains may be limited to short distances due to frustration associated with inhomogeneities in the structure and/or local composition. This also agrees reasonably with the inclusion of constant phase element (CPE) wherein the dynamical origin is involved [45,47-50].

# 4. Conclusion

Analysis of phase equilibria within the BMT system revealed processing parameters that stabilise the pyrochlore phase with the desired properties. The established composition-structure-property relationships offer valuable insights into the practical application of BMT pyrochlores. Significantly, these pyrochlores demonstrate exceptional dielectric properties, including  $\varepsilon'$  values ranging from 73 to 84, low tan  $\delta$  (in the order of  $10^{-3}$ ) and high activation energies (approximately 1.10–1.49 eV). Furthermore, dielectric performance is influenced by the interplay of composition, microstructure and processing control; therefore, understanding these parameters is critical for advancing knowledge and enabling the tailored synthesis of BMT pyrochlores for specific electrical applications.

# CRediT authorship contribution statement

K.B. Tan: Writing – review & editing, Validation, Supervision, Resources, Project administration, Methodology, Formal analysis, Conceptualization. P.Y. Tan: Writing – original draft, Software, Methodology, Investigation, Formal analysis, Data curation. Y. Feng: Visualization, Software, Methodology. C.C. Khaw: Supervision, Resources, Methodology, Conceptualization. V. Raman: Visualization, Validation, Resources. H.C. Ananda Murthy: Validation, Software, Investigation.

**R. Balachandran:** Validation, Resources, Data curation. **S.K. Chen:** Supervision, Methodology, Formal analysis. **O.J. Lee:** Visualization, Software, Investigation. **K.Y. Chan:** Validation, Methodology, Formal analysis. **D. Zhou:** Writing – review & editing, Visualization, Software, Methodology. **M. Lu:** Visualization, Methodology, Formal analysis.

### **Declaration of competing interest**

The authors declare that they have no known competing financial interests or personal relationships that could have appeared to influence the work reported in this paper.

#### Acknowledgement

The financial supports from the Ministry of Higher Education, Malaysia via the Fundamental Research Grant Scheme (FRGS/1/2020/STG05/UPM/02/2) and Putra Graduates Initiative Grant (GP-IPS-2023/9773100) are gratefully acknowledged. Also, special thanks are dedicated to the powder XRD data via STOE STADI-P diffractometer and technical advices from Prof. A. R. West, School of Chemical, Materials and Biological Engineering, The University of Sheffield, UK.

### Appendix A. Supplementary data

Supplementary data to this article can be found online at https://doi.org/10.1016/j.jsamd.2025.100866.

#### References

- Q. Yin, B. Zhu, H. Zeng, Microstructure, Property and Processing of Functional Ceramics, Springer, Heidelberg, 2010, https://doi.org/10.1007/978-3-642-01694-3
- [2] Anthony R. West, Solid State Chemistry and its Applications, second ed., John Wiley & Sons, Ltd., Oxford, 2022.
- [3] M.A. Subramanian, G. Aravamudan, G.V. Subba Rao, Oxide pyrochlores: a review, Prog. Solid State Chem. 15 (1983) 55–143, https://doi.org/10.1016/0079-6786 (83)00001-8
- [4] D.P. Cann, C.A. Randall, T.R. Shrout, Investigation of the dielectric properties of bismuth pyrochlores, Solid State Commun. 100 (1996) 529–534, https://doi.org/ 10.1016/0038-1098(96)00012-9
- [5] A. Mergen, W.E. Lee, Crystal chemistry, thermal expansion and dielectric properties of (Bi<sub>1.5</sub>Zn<sub>0.5</sub>)(Sb<sub>1.5</sub>Zn<sub>0.5</sub>)O<sub>7</sub> pyrochlore, Mater. Res. Bull. 32 (1997) 175–189, https://doi.org/10.1016/s0025-5408(96)00186-9.
- [6] G.C. Miles, A.R. West, Pyrochlore phases in the system ZnO-Bi<sub>2</sub>O<sub>3</sub>-Sb<sub>2</sub>O<sub>5</sub>: I. stoichiometries and phase equilibria, J. Am. Ceram. Soc. 89 (2006) 1042–1046, https://doi.org/10.1111/j.1551-2916.2005.00799.x.
- K.B. Tan, C.K. Lee, Z. Zainal, G.C. Miles, A.R. West, Stoichiometry and doping mechanism of the cubic pyrochlore phase in the system Bi2O3-ZnO-Nb2O5,
   J. Mater. Chem. 15 (2005) 3501–3506, https://doi.org/10.1039/b505803c.
- [8] K.B. Tan, C.C. Khaw, C.K. Lee, Z. Zinal, Y.P. Tan, H. Shaari, High temperature impedance spectroscopy study of non-stoichiometric bismuth zinc niobate pyrochlore, Mater. Sci. Poland 27 (3) (2009) 825–837, https://doi.org/10.1016/j. ceramint.2008.08.006.
- [9] C.C. Khaw, C.K. Lee, Z. Zainal, G.C. Miles, A.R. West, Pyrochlore phase formation in the system Bi<sub>2</sub>O<sub>3</sub>-ZnO-Ta<sub>2</sub>O<sub>5</sub>, J. Am. Ceram. Soc. 90 (2007) 2900–2904, https:// doi.org/10.1111/j.1551-2916.2007.01608.x.
- [10] P.Y. Tan, K.B. Tan, C.C. Khaw, Z. Zainal, S.K. Chen, M.P. Chon, Phase equilibria and dielectric properties of Bi<sub>3+(5/2)x</sub>Mg<sub>2-x</sub>ND<sub>3-(3/2)x</sub>O<sub>14-x</sub> cubic pyrochlores, Ceram. Int. 40 (3) (2014) 4237–4246, https://doi.org/10.1016/j. ceramint 2013 08 087
- [11] N.A.M. Dasin, K.B. Tan, C.C. Khaw, Z. Zainal, S.K. Chen, Subsolidus solution and electrical properties of Sr-substituted bismuth magnesium niobate pyrochlores, Ceram. Int. 43 (13) (2017) 10183–10191, https://doi.org/10.1016/j. ceramint.2017.05.043.
- [12] I. Levin, T.G. Amos, J.C. Nino, T.A. Vanderah, C.A. Randall, M.T. Lanagan, Structural study of an unusual cubic pyrochlore Bi<sub>1.5</sub>Zn<sub>0.92</sub>Nb<sub>1.5</sub>O<sub>6.92</sub>, J. Solid State Chem. 168 (2002) 69–75, https://doi.org/10.1006/jssc.2002.9681.
- [13] J.C. Nino, M.T. Lanagan, C.A. Randall, Dielectric relaxation in Bi<sub>2</sub>O<sub>3</sub>-ZnO-Nb<sub>2</sub>O<sub>5</sub> cubic pyrochlore, J. Appl. Phys. 89 (8) (2001) 4512–4516, https://doi.org/10.1063/1.1357468.
- [14] M. Valant, P.K. Davies, Crystal chemistry and dielectric properties of chemically substituted (Bi<sub>1.5</sub>Zn<sub>1.0</sub>Nb<sub>1.5</sub>)O<sub>7</sub> and Bi<sub>2</sub>(Zn<sub>2/3</sub>Nb<sub>4/3</sub>)O<sub>7</sub> pyrochlores, J. Am. Ceram. Soc. 83 (1) (2000) 147–153, https://doi.org/10.1111/j.1151-2916.2000.tb01163.
- [15] R.L. Withers, T.R. Welberry, A.K. Larsson, Y. Liu, L. Noren, H. Rundlof, F.J. Brink, Local crystal chemistry, induced strain and short range order in the cubic

- pyrochlore  $(Bi_{1.5-a}Zn_{0.5-p})(Zn_{0.5-p}Nb_{1.5-a})O_{(7-1.5a-\beta-\gamma-2.5a)}$  (BZN), J. Solid State Chem. 177 (1) (2004) 231–244, https://doi.org/10.1016/j.jssc.2003.07.005.
- [16] F.A. Jusoh, K.B. Tan, Z. Zainal, S.K. Chen, C.C. Khaw, O.J. Lee, Novel pyrochlores in the Bi<sub>2</sub>O<sub>3</sub>-Fe<sub>2</sub>O<sub>3</sub>-Ta<sub>2</sub>O<sub>5</sub> (BFT) ternary system: synthesis, structural and electrical properties, J. Mater. Res. Technol. 9 (5) (2020) 11022–11034, https://doi.org/ 10.1016/j.jmrt.2020.07.102.
- [17] F.A. Jusoh, K. B Tan, Z. Zainal, S.K. Chen, C.C. Khaw, O.J. Lee, Investigation of structural and dielectric properties of subsolidus bismuth iron niobate pyrochlores, J. Asian Ceram. Soc. 8 (3) (2020) 957–969, https://doi.org/10.1080/ 21870764.2020.1799914.
- [18] N.A.M. Dasin, K.B. Tan, C.C. Khaw, Z. Zainal, O.J. Lee, S.K. Chen, Doping mechanisms and dielectric properties of Ca-doped bismuth magnesium niobate pyrochlores, Mater. Chem. Phys. 242 (2020) 122558, https://doi.org/10.1016/j. matchemphys.2019.122558.
- [19] M.W. Lufaso, T.A. Vanderah, I.M. Pazos, I. Levin, R.S. Roth, J.C. Nino, et al., Phase formation, crystal chemistry and properties in the system Bi<sub>2</sub>O<sub>3</sub>-Fe<sub>2</sub>O<sub>3</sub>-Nb<sub>2</sub>O<sub>5</sub>, J. Solid State Chem. 179 (2006) 3900–3910, https://doi.org/10.1016/j. issc.2006.08.036.
- [20] M. Valant, D. Suvorov, The Bi<sub>2</sub>O<sub>3</sub>-Nb<sub>2</sub>O<sub>5</sub>-NiO phase diagram, J. Am. Ceram. Soc. 88 (2005) 2540–2543, https://doi.org/10.1111/j.1551-2916.2005.00439.x.
- [21] M.P. Chon, K.B. Tan, C.C. Khaw, Z. Zainal, Y.H. Taufiq Yap, P.Y. Tan, Synthesis, structural and electrical properties of novel pyrochlores in the Bi<sub>2</sub>O<sub>3</sub>-CuO-Ta<sub>2</sub>O<sub>5</sub> ternary system, Ceram. Int. 38 (2012) 4253–4261, https://doi.org/10.1016/j.ceramint 2012 02 007
- [22] T.A. Vanderah, T. Siegrist, M.W. Lufaso, M.C. Yeager, R.S. Roth, J.C. Nino, et al., Phase formation and properties in the system Bi<sub>2</sub>O<sub>3</sub>:2CoO<sub>1+x</sub>:Nb<sub>2</sub>O<sub>5</sub>, Eur. J. Inorg. Chem. 23 (2006) 4908–4914, https://doi.org/10.1002/ejic.200600661.
- [23] T.A. Vanderah, M.W. Lufaso, A.U. Adler, I. Levin, J.C. Nino, V. Provenzano, Subsolidus phase equilibria and properties in the system Bi<sub>2</sub>O<sub>3</sub>:Mn<sub>2</sub>O<sub>3±x</sub>:Nb<sub>2</sub>O<sub>5</sub>, J. Solid State Chem. 179 (2006) 3467–3477, https://doi.org/10.1016/j. issr 2006 07 014
- [24] K.B. Tan, M.P. Chon, C.C. Khaw, Z. Zainal, Y.H. Taufiq-Yap, S.K. Chen, P.Y. Tan, Phase equilibria in the Bi<sub>2</sub>O<sub>3</sub>-CuO-Nb<sub>2</sub>O<sub>5</sub> ternary system, Ceram. Int. 43 (6) (2017) 4930–4936, https://doi.org/10.1016/j.ceramint.2016.12.147.
- [25] M.P. Chon, K.B. Tan, C.C. Khaw, Z. Zainal, Y.H. Taufiq-Yap, S.K. Chen, P.Y. Tan, Subsolidus phase equilibria and electrical properties of pyrochlores in the Bi<sub>2</sub>O<sub>3</sub>-CuO-Ta<sub>2</sub>O<sub>5</sub> ternary system, J. Alloys Compd. 675 (2016) 116–127, https://doi.org/ 10.1016/j.iallcom.2016.03.089.
- [26] C.C. Khaw, K.B. Tan, C.K. Lee, A.R. West, Phase equilibria and electrical properties of pyrochlore and zirconolite phases in the Bi<sub>2</sub>O<sub>3</sub>-ZnO-Ta<sub>2</sub>O<sub>5</sub> system, J. Eur. Ceram. Soc. 32 (3) (2012) 671–680, https://doi.org/10.1016/j. ieurceramsoc.2011.10.012.
- [27] M.P. Chon, K.B. Tan, Z. Zainal, Y.H. Taufiq-Yap, Y.P. Tan, C.C. Khaw, S.K. Chen, Synthesis and electrical properties of Zn-substituted bismuth copper tantalate pyrochlores, Int. J. Appl. Ceram. Technol. 13 (2016) 718–725, https://doi.org/ 10.1111/jiac.12547.
- [28] B. Shen, X. Yao, D. Peng, L. Kang, Structure and dielectric properties of Bi<sub>2</sub>O<sub>3</sub>-ZnO-CaO-Ta<sub>2</sub>O<sub>5</sub> ceramics, Ceram. Int. 30 (7) (2004) 1207–1210, https://doi.org/10.1016/j.ceramint.2003.12.081.
- [29] P.Y. Tan, K.B. Tan, C.C. Khaw, Z. Zainal, S.K. Chen, M.P. Chon, Structural and electrical properties of bismuth magnesium tantalate pyrochlores, Ceram. Int. 38 (2012) 5401–5409, https://doi.org/10.1016/j.ceramint.2012.03.050.
- [30] N.A. Zhuk, M.G. Krzhizhanovskaya, Thermal expansion of bismuth magnesium tantalate and niobate pyrochlores, Ceram. Int. 47 (2021) 30099–30105, https://doi.org/10.1016/j.ceram.int.2021.07.187
- [31] N.A. Zhuk, M.G. Krzhizhanovskaya, A.V. Koroleva, N.A. Sekushin, S.V. Nekipelov, V.V. Kharton, B.A. Makeev, V.P. Lutoev, Y.D. Sennikova, Cu, Mg co-doped bismuth tantalate pyrochlores: crystal structure, XPS spectra, thermal expansion, and electrical properties, Inorg. Chem. 61 (10) (2022) 4270–4282, https://doi.org/10.1021/acs.inorgchem.1c03053.

- [32] N.A. Zhuk, M.G. Krzhizhanovskaya, A.V. Koroleva, S.V. Nekipelov, D.V. Sivkov, V. N. Sivkov, A.M. Lebedev, R.G. Chumakov, B.A. Makeev, V.V. Kharton, V.V. Panova, R.I. Korolev, Spectroscopic characterisation of cobalt doped bismuth tantalate pyrochlore, Solid State Sci. 125 (2022) 106820, https://doi.org/10.1016/j.solidstatesciences.2022.106820.
- [33] N.A. Zhuk, M.G. Krzhizhanovskaya, N.A. Sekushin, D.V. Sivkov, I. E. Abdurakhmanov, Crystal structure, dielectric and thermal properties of cobalt doped bismuth tantalate pyrochlore, J. Mater. Res. Technol. 22 (2023) 1791–1799, https://doi.org/10.1016/j.jmrt.2022.12.059.
- [34] N.A. Zhuk, M.G. Krzhizhanovskaya, A.V. Koroleva, A.A. Reveguk, D.V. Sivkov, S. V. Nekipelov, Thermal expansion, crystal structure, XPS and NEXAFS spectra of Fedoped bismuth tantalate pyrochlore, Ceram. Int. 48 (10) (2022) 14849–14855, https://doi.org/10.1016/j.ceramint.2022.02.021.
- [35] R.D. Shannon, Revised effective ionic radii and systematic studies of interatomic distances in halides and chalcogenides, Acta Cryst A32 (1976) 751–767, https:// doi.org/10.1107/s0567739476001551.
- [36] C.D. Ling, R.L. Withers, S. Schmid, J.G. Thompson, A review of bismuth-rich binary oxides in the systems Bi<sub>2</sub>O<sub>3</sub>-Nb<sub>2</sub>O<sub>5</sub>, Bi<sub>2</sub>O<sub>3</sub>-Ta<sub>2</sub>O<sub>5</sub>, Bi<sub>2</sub>O<sub>3</sub>-MoO<sub>3</sub>, and Bi<sub>2</sub>O<sub>3</sub>-WO<sub>3</sub>, J. Solid State Chem. 137 (1998) 42–61, https://doi.org/10.1006/jssc.1997.7677.
- [37] W. Zhou, Structural chemistry and physical properties of some ternary oxides in the Bi<sub>2</sub>O<sub>3</sub>-Ta<sub>2</sub>O<sub>5</sub> system, J. Solid State Chem. 101 (1992) 1–17, https://doi.org/ 10.1006/jssc.1997.7677.
- [38] Y. Baskin, D.C. Schell, Phase studies in the binary system MgO-Ta<sub>2</sub>O<sub>5</sub>, J. Am. Ceram. Soc. 46 (1963) 174–177, https://doi.org/10.1111/j.1151-2916.1963.
- [39] R.C. Ropp, R. C, Group 5 (V, Nb, Ta) alkaline earth compounds, in: Encyclopedia of the Alkaline Earth Compounds, Newnes, 2012, pp. 701–794, https://doi.org/ 10.1016/b978-0-444-59550-8.00009-0. Elsevier.
- [40] A.P. Pivovarova, Compound Mg<sub>2</sub>Ta<sub>2</sub>O<sub>7</sub> and its interaction with Nd<sub>3</sub>TaO<sub>7</sub>, Refract. Ind. Ceram. 43 (2002) 172–175, https://doi.org/10.1023/a:1020567016907.
- [41] N. Djordjević, Influence of Bi<sub>2</sub>O<sub>3</sub> on sintering and crystallisation of cordierite ceramics, Sci. Sinter. 37 (2005) 189–197, https://doi.org/10.2298/sos0503189d.
- [42] H.A. Harwig, A.G. Gerards, The polymorphism of bismuth sesquioxide, Thermochim. Acta 28 (1979) 121–131, https://doi.org/10.1016/0040-6031(79) 87011-2.
- [43] A.P. Chernyshev, V.A. Petrov, V.E. Titov, A.Y. Vorobyev, Thermal radiative properties of magnesium oxide at high temperatures, Thermochim. Acta 218 (1993) 195–209, https://doi.org/10.1016/0040-6031(93)80422-7.
- [44] D.A. Reeve, The binary system CaO-Ta<sub>2</sub>O<sub>5</sub>, J. Less-Common Met. 17 (1969) 215–222, https://doi.org/10.1016/0022-5088(69)90055-1.
- [45] P.Y. Tan, K.B. Tan, C.C. Khaw, H.C. Ananda Murthy, R. Balachandran, S.K. Chen, O.J. Lee, K.Y. Chan, M. Lu, Electrical circuit modeling for the relaxor response of bismuth magnesium tantalate pyrochlore, J. Sci.: Adv. Mater. Devices 9 (2) (2024) 100715. https://doi.org/10.1016/j.isamd.2024.100715.
- [46] M.A.L. Nobre, S. Lanfredi, Dielectric properties of Bi<sub>3</sub>Zn<sub>2</sub>Sb<sub>3</sub>O<sub>14</sub> ceramics at high temperature, Mater. Lett. 47 (2001) 362–366, https://doi.org/10.1016/s0167-577x(00)00267-6.
- [47] P.Y. Tan, K.B. Tan, C.C. Khaw, Z. Zainal, S.K. Chen, O.J. Lee, M.P. Chon, Non-ferroelectric relaxor properties of BMN, Bi<sub>3.55</sub>Mg<sub>1.78</sub>Nb<sub>2.67</sub>O<sub>13.78</sub> pyrochlore, J. Alloys Compd. 816 (2020) 152576, https://doi.org/10.1016/j.iallcom.2019.152576.
- [48] R.A.M. Osman, N. Masó, A.R. West, Bismuth zinc niobate pyrochlore, a relaxor-like non-ferroelectric, J. Am. Ceram. Soc. 95 (2012) 296–302, https://doi.org/ 10.1111/i.1551-2916.2011.04779.x.
- [49] R.A.M. Osman, A.R. West, Electrical characterisation and equivalent circuit analysis of (Bi<sub>1.5</sub>Zn<sub>0.5</sub>)(Nb<sub>0.5</sub>Ti<sub>1.5</sub>)O<sub>7</sub> pyrochlore, a relaxor ceramic, J. Appl. Phys. 109 (2011) 074106, https://doi.org/10.1063/1.3553883.
- 109 (2011) 074106, https://doi.org/10.1063/1.3553883.
  [50] N.R. McLaren, M.C. Ferrarelli, Y.W. Tung, D.C. Sinclair, A.R. West, Synthesis, structure and electrical properties of Cu<sub>3.21</sub>Ti<sub>1.16</sub>Nb<sub>2.63</sub>O<sub>12</sub> and the CuO<sub>x</sub>-TiO<sub>2</sub>-Nb<sub>2</sub>O<sub>5</sub> pseudoternary phase diagram, J. Solid State Chem. 184 (2011) 1813–1819, https://doi.org/10.1016/j.jssc.2011.05.032.